J. Fluid Mech. (2010), *vol.* 658, *pp.* 279–293.
doi:10.1017/S0022112010001709

Numerical modelling of finite-amplitude electro-thermo-convection in a dielectric liquid layer subjected to both unipolar injection and temperature gradient

PH. TRAORÉ[1]†, A. T. PÉREZ[2], D. KOULOVA[3] AND H. ROMAT[1]

[1]Laboratoire d'Etudes Aérodynamiques, Boulevard Pierre et Marie Curie, BP 30179, 86962 Futuroscope-Chasseneuil, France

[2]Departamento de Electrónica y Electromagnetismo, Facultad de Física, Avenida Reina Mercedes s/n, 41012 Sevilla, Spain

[3]Institute of Mechanics, Bulgarian Academy of Sciences, 1113 Sofia, Bulgaria

(Received 4 February 2008; revised 2 March 2010; accepted 7 April 2010; first published online 6 July 2010)

In this paper, we solve numerically the entire set of equations associated with the electro-thermo-convective phenomena that take place in a planar layer of dielectric liquid heated from below and subjected to unipolar injection. For the first time the whole set of coupled equations is solved: Navier–Stokes equations, electrohydrodynamic (EHD) equations and the energy equation. We first validate the numerical simulation by comparing the electro-convection stability criteria with ones obtained with a stability approach. The numerical solution of the electro-thermo-convection problem is then presented entirely with a detailed analysis of stability parameters. In particular, the relation between fluid velocity, non-dimensional electrical parameter T, Rayleigh number Ra and Prandtl number Pr is given. An analytical model is presented in order to understand the flow behaviour at some critical conditions. The way that the onset of motion passes from purely electrical convection to purely thermal convection is, in particular, investigated and explained in detail. Finally, a result on the heat transfer enhancement due to electro-convection is exhibited and compared with data from experimental works available in this field.

Key words: cavities, instability, MHD and electrohydrodynamics

1. Introduction

Electro-convective phenomena in dielectric liquids have already been widely investigated over the last four or five decades. It is well known that the flow in an isothermal dielectric liquid layer between two infinite parallel electrodes (with one raised to a high potential) is due to the action of the electric field on the electric charges injected into the liquid. The electrochemical mechanisms giving rise to the injection of charges at the interface between the dielectric liquid and the electrodes have also been studied in depth by Felici (1972). The injection phenomenon is generated by

† Email address for correspondence: philippe.traore@univ-poitiers.fr

positive and negative electrodes submerged in liquids of low enough conductivity and is called unipolar injection when it occurs at only one electrode.

In electrohydrodynamics (EHD) the convection induced by charge injection in a dielectric liquid is a problem as fundamental as the Rayleigh–Bénard problem in non-isothermal fluid mechanics. The action of the electric field on the space charge density arising from unipolar injection has the same destabilizing role as the thermal field when the fluid is heated from below in the Rayleigh–Bénard problem. In electro-convection the flow originates from the growth of instabilities triggered by the critical value of the non-dimensional electrical parameter T (Atten & Moreau 1972) whereas in Rayleigh–Bénard convection the instabilities are triggered by the critical value of the Rayleigh number Ra. However, the two convections are not identical from a physical point of view. The mechanisms at the origin of the motion of the fluid are quite different in both cases: in Rayleigh–Bénard convection, the heat transfer is governed by thermal diffusion whereas the migration of ions is the relevant mechanism in the electric charge transfer in electro-convection.

In 1969 Felici was the first to propose a simple isothermal hydraulic model in which inertial effects are neglected and for which injection is unipolar and weak. A convective roll cell was modelled by two columns of the same radius with constant liquid velocity. His model explains in qualitative terms the onset and persistence of the steady finite-amplitude motion of two-dimensional rolls in an initially static plane layer of dielectric fluid. The author established the existence of two criteria, the standard stability criterion T_c associated with the perturbation of infinitely small amplitudes and another criterion $T_f (T_f < T_c)$ corresponding to finite-amplitude velocity disturbances.

The combined effects of an electric field and a thermal gradient simultaneously applied to a horizontal dielectric liquid layer leads to complex physical interactions in the flow and have received much attention in recent years (Castellanos, Atten & Velarde 1984*a*; Atten, McCluskey & Pérez 1988; McCluskey, Atten & Pérez 1991). One of the reasons for this interest is that the development of electro-thermo-convective instabilities in liquids could be a promising way to increase the heat transfer by means of electrical forces. Such combined effects are therefore worthy of examination not only from a fundamental point of view but also because of potential technological advantages that may result from them (Bryan & Seyed-Yagoobi 1997, 2001; Lin & Jang 2005; Grassi & Testi 2006; Suman 2006). The stability analysis was done in a series of papers by Worraker & Richardson (1979, 1981), Martin & Richardson (1982), Castellanos *et al.* (1984*a*,*b*), Rodriguez, Castellanos & Richardson (1986) and Pontiga & Castellanos (1992, 1994). A first attempt to incorporate temperature effects in the hydraulic model of Felici (1969) was made by Martin (1982). Richardson (1988) made a more complete study of Felici's model.

Since the solution of the governing electro-thermo-hydrodynamic (ETHD) equations is not readily amenable to an exact mathematical analysis, this problem has been tackled by several alternative methods. Only a few numerical simulations have been attempted on pure EHD convection problems (Castellanos, Atten & Pérez 1987; Chicón, Castellanos & Martín 1997; Chicón, Castellanos & Pérez 1999; Vázquez, Georghiou & Castellanos 2006, 2008; Tsai *et al.* 2007). To our knowledge, a direct and fully coupled numerical simulation of the ETHD problem has never been performed in a satisfactory way. In the present work, we carry out a direct numerical study of electro-thermo-convection in a two-dimensional cavity.

The present paper is organized as follows. In § 2, we define the mathematical problem to be studied. Section 3 is devoted to a brief presentation of the numerical method that we developed to compute the dynamic, electrical and thermal variables

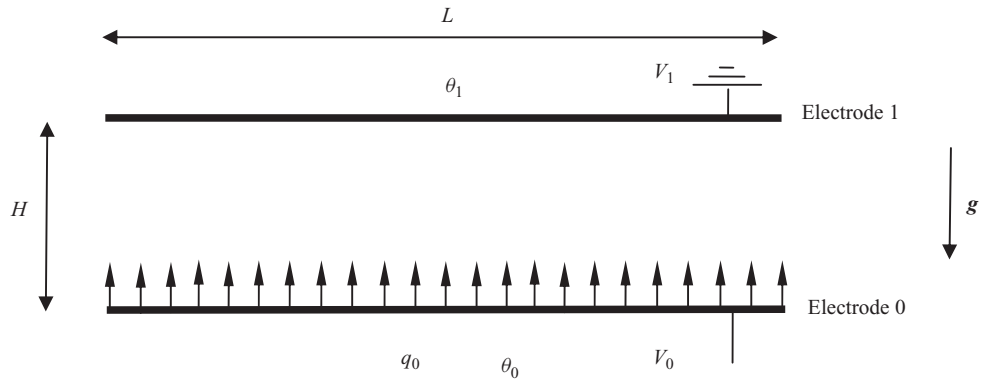

FIGURE 1. The dielectric liquid layer.

describing the problem. Accurate quantitative results concerning the transition to convection are provided in § 4. Also in this section an analytical model is presented that helps to understand the different types of bifurcation encountered. Finally, in § 5, we quantify the real impact of electro-convection on heat transfer and compare our numerical data with experimental results. In § 6 we present our conclusions.

2. Statement of the problem

2.1. *Governing equations*

Consider an incompressible and perfectly insulating liquid of density ρ, permittivity ε, constant kinematic viscosity ν and constant thermal diffusivity κ, enclosed between two parallel planar electrodes. These horizontal metallic electrodes (figure 1) are assumed to be rigid heat conducting plates and maintained respectively at fixed temperatures θ_0 and θ_1. The emitter electrode corresponding to the plane $y = 0$ is held at potential V_0 and is the source of ions which are injected into the liquid and collected by the electrode at $y = H$ which is held at potential V_1. The injection of unipolar charge of mobility K at the emitter is assumed 'homogeneous' and 'autonomous'; this means that $q = q_0$ at $y = 0$ at all times since the injector, and hence the injection rate are not influenced by perturbation in the bulk. Furthermore, in order to avoid undue complexity, we neglect the charge diffusion process and Joule heating, and make use of the Boussinesq approximation.

In this paper, we consider the case of strong injection. In this context, experiments have shown a weak influence of the temperature gradient on electro-convection regimes (Pérez *et al.* 1988; Atten *et al.* 1988). Also, Rodriguez *et al.* (1986) have shown that the influence on the stability threshold of the variation of mobility and permittivity with temperature is negligible. Therefore the liquid properties will be taken as independent of temperature.

If now length, time, liquid velocity, charge density, electric potential, electric field temperature, pressure field, mass density, permittivity and ionic mobility are made dimensionless by making the following transformations:

$$x_i^* = \frac{x_i}{H}, \quad t_0 = \frac{H^2}{\nu}, \quad u_i^* = \frac{u_i}{\nu/H}, \quad q^* = \frac{q}{q_0}, \quad V^* = \frac{V}{(V_0 - V_1)}, \quad E_i^* = \frac{E_i}{(V_0 - V_1)/H},$$

$$\theta^* = \frac{\theta}{(\theta_0 - \theta_1)}, \quad p^* = \frac{p}{\rho_0(\nu/H)^2}, \quad \rho^* = \frac{\rho}{\rho_0}, \quad \varepsilon^* = \frac{\varepsilon}{\varepsilon_0}, \quad K^* = \frac{K}{K_0},$$

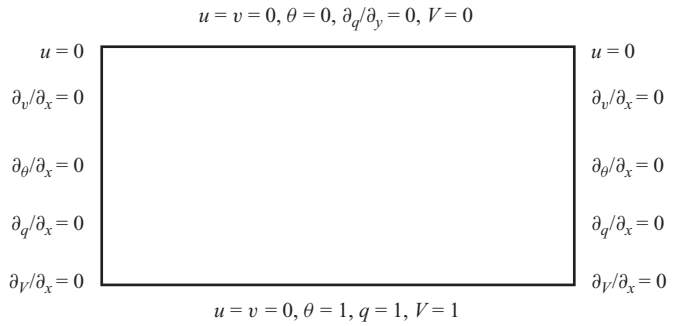

FIGURE 2. Boundary conditions.

the resulting governing equations of this thermo-electrohydrodynamic system are

$$\nabla \cdot \boldsymbol{u} = 0, \tag{1}$$

$$\frac{\partial \boldsymbol{u}}{\partial t} + (\boldsymbol{u} \cdot \nabla)\boldsymbol{u} = -\nabla \tilde{p} + \Delta \boldsymbol{u} + RTCq\boldsymbol{E} + \frac{Ra}{Pr}\theta \boldsymbol{e}_z, \tag{2}$$

$$\frac{\partial \theta}{\partial t} + \boldsymbol{u} \cdot \nabla \theta = \frac{1}{Pr}\Delta \theta, \tag{3}$$

$$\frac{\partial q}{\partial t} + \nabla \cdot (q(\boldsymbol{u} + R\boldsymbol{E})) = 0, \tag{4}$$

$$\Delta V = -Cq, \tag{5}$$

$$\boldsymbol{E} = -\nabla V. \tag{6}$$

The Rayleigh number Ra, applied voltage measure T, injection strength C, mobility parameter M, electrical Reynolds number R and Prandtl number Pr are defined by

$$\left.\begin{aligned} Ra = \frac{g\beta \Delta\theta H^3}{\nu\kappa}, \quad T = \frac{\varepsilon_0 \Delta V}{\rho_0 \nu \quad K_0}, \quad C = \frac{q_0 H^2}{\varepsilon_0 \Delta V}, \\ M = \frac{1}{K_0}\left(\frac{\varepsilon_0}{\rho_0}\right)^{1/2}, \quad R = \frac{T}{M^2}, \quad Pr = \frac{\nu}{\kappa}. \end{aligned}\right\} \tag{7}$$

2.2. *Boundary conditions*

Horizontal walls with no-slip conditions are assumed impermeable as well as thermally and electrically perfectly conducting. Thus the associated boundary conditions on velocity, temperature, electric potential and charge density are chosen as shown in figure 2. On lateral walls we apply symmetrical boundary conditions, essentially used to simulate an infinitely long cavity.

3. Numerical solution method

The problem under consideration is described mathematically by the conservation equations for mass, momentum, energy and charge density and by Poisson's equation for potential. The above set of coupled partial differential equations (see (1)–(6)) is discretized using a finite-volume approach. All the details on the finite-volume discretization method used here are given by Patankar (1980).

Considering the hyperbolic nature of the transport equation for charge density q, since diffusion has been neglected steep gradients may appear. For this kind of equation, the 'central difference scheme' (CDS) is known to introduce undesirable

over- and undershoots while the 'upwind difference scheme' (UDS) will smear the solution in an unacceptable way.

So, because of the lack of physical diffusion and to prevent the development of these possible oscillations of the solution, one has to add artificial or numerical viscosity and also use a non oscillating, non diffusive and bounded scheme (Godunov 1959) or schemes which have the total variation diminishing (TVD) property (Davis 1984). In order to satisfy these unavoidable requirements, we have chosen the second-order smooth monotonic algorithm for real transport (SMART) scheme of Gaskell & Lau (1988).

Since the momentum equations are written for an incompressible fluid, the main difficulty lies in the computation of pressure from velocity. We chose the Augmented Lagrangian method (Fortin & Glowinsky 1983) as velocity–pressure coupling algorithm. All details of the implementation can be found in Traoré (1996).

4. Small- and finite-amplitude instability

4.1. *Analytical qualitative analysis of the bifurcation*

A liquid layer heated from below becomes unstable at a certain critical value of the Rayleigh number. When injection is present, a combination of Ra and T gives the threshold for instability. Before presenting the numerical results, it is useful to have some analytical insight. In the spirit of the hydraulic model of Felici (1969), or other semi-analytical methods as described in Castellanos (1991), we can average the equation of motion over a convective cell (a similar approach can be found in Richardson 1988). Let us assume a given profile of velocity $\boldsymbol{u} = A\boldsymbol{u}_0(x, z)$ and multiply (2) by $\boldsymbol{u}_0$. Integrating over a convective cell we have

$$C\frac{T^2}{M^2}\int q\boldsymbol{E}\cdot\boldsymbol{u}_0 \mathrm{d}\tau + \frac{Ra}{Pr}\int \theta \boldsymbol{e}_z\cdot\boldsymbol{u}_0 \mathrm{d}\tau + \int \boldsymbol{u}_0\cdot\nabla^2\boldsymbol{u}\,\mathrm{d}\tau = 0, \tag{8}$$

where the inertial term is neglected, the pressure term is zero after integration, and a steady state is assumed. To carry out the integration we need the profiles of temperature θ and charge q. These can be computed to any order in amplitude A if we use a very simplified velocity profile: the cell is divided into two columns of width $L/2$ and the liquid goes up with uniform velocity A in one column and goes down with uniform velocity $-A$ in the other. This corresponds to taking $\boldsymbol{u}_0 = -1$ for $0 < x < L/2$ and $\boldsymbol{u}_0 = 1$ for $L/2 < x < L$. The charge density in the rising column is given by

$$q = \frac{1}{\left(1 + C\dfrac{z}{1 \pm M^2 A/T}\right)}, \tag{9}$$

where the + sign corresponds to the right column and the − sign to the left one.

This expression is valid as long as $A < T/M^2$. When the velocity approaches T/M^2, the charge on the returning column tends to zero and the electric driving term saturates at a value proportional to T^2. The electrical term has the qualitative dependence on A depicted in figure 3(a) (see Felici 1969). Close to $A = 0$, the function is concave. There is a rapid increase with A and then a saturation for $A > T/M^2$.

The temperature profile in each column follows from (3) with a constant velocity u_{0z}. The buoyancy term becomes,

$$\frac{Ra}{Pr}\int \theta \boldsymbol{e}_z\cdot\boldsymbol{u}_0 \mathrm{d}\tau = \frac{Ra\,L_x}{2Pr}\left(\frac{\sinh(APr)}{\cosh(APr)-1} - \frac{2}{APr}\right). \tag{10}$$

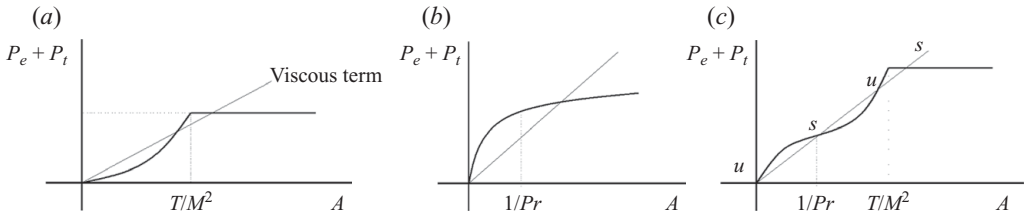

FIGURE 3. Evolution of the driven term $P_e + P_t$ as a function of A. (a) P_e dominates, (b) P_t dominates and (c) P_t dominates for small A.

Unlike the electrical term, near $A \sim 0$, the function is convex. However, it also tends to saturate for $A \gg 1/Pr$. Figure 3(b) represents qualitatively the dependence of the thermal term P_t on the velocity amplitude A.

Collecting the different terms, expanding up to order A^3, and rearranging, equation (8) can be expressed as

$$\left(\frac{Ra}{Ra_c} + \frac{T}{T_c}\right) + \left(\frac{M^4}{T_c T} - \frac{RaPr^2}{60Ra_c}\right) A^2 = 1. \tag{11}$$

For $A = 0$, this equation provides the instability threshold in the Ra–T plane. The subcritical or supercritical character of the bifurcation is determined by the coefficient of A^2. For the Rayleigh–Bénard problem, in the absence of electric forces, the instability develops as a supercritical bifurcation. The behaviour is totally different in the electrohydrodynamic instability (see e.g. Castellanos 1991), as the bifurcation is subcritical. The liquid is at rest until T exceeds T_c, then the system evolves towards a motion with a velocity that is not of small amplitude, and cannot be predicted by a quasi-linear analysis (Felici 1969; Atten & Lacroix 1979). Once the convective regime is established, decreasing the value of T below the instability threshold does not result in the suppression of motion until a second value of T, the finite-amplitude criterion, is reached. Therefore, a hysteresis loop associated with these two values of the stability parameter T results.

If the combination $RaPr^2$ is smaller than a certain value one expects to observe a subcritical bifurcation and a behaviour of the electric type: there will be two instability thresholds, one associated with the instability of small-amplitude perturbations and a second associated with the suppression of the finite-amplitude solution (see figure 3a).

If Pr is high enough to make the coefficient of A^2 negative, the curvature of the total driving force is dominated by the thermal term near $A = 0$. However, for $A \gg 1/Pr$ the thermal term saturates, and the whole driving force $P_e + P_t$ acquires the curvature of the electrical term (figure 3c). Near the critical value of T we will have a supercritical bifurcation, but as T increases, a situation with four possible solutions is found. Of these four solutions, two are unstable and two are stable. They are labelled '***u***' and '***s***', respectively, in the plot. In this case there are three critical values. The first is the small-amplitude critical value T_c, which corresponds to the appearance of the first stable equilibrium. The second critical value, labelled T_f, is associated with the appearance of the second stable point in figure 3(c). The third critical value corresponds to the disappearance of the first stable point in figure 3(c) and represents a second small-amplitude critical value, labelled T_{c2}. This value is always greater than T_f and T_c.

4.2. *Ra–T diagram*

We have studied numerically the instability problem in detail, focusing on an understanding of the role played by the main non-dimensional parameters Ra and T.

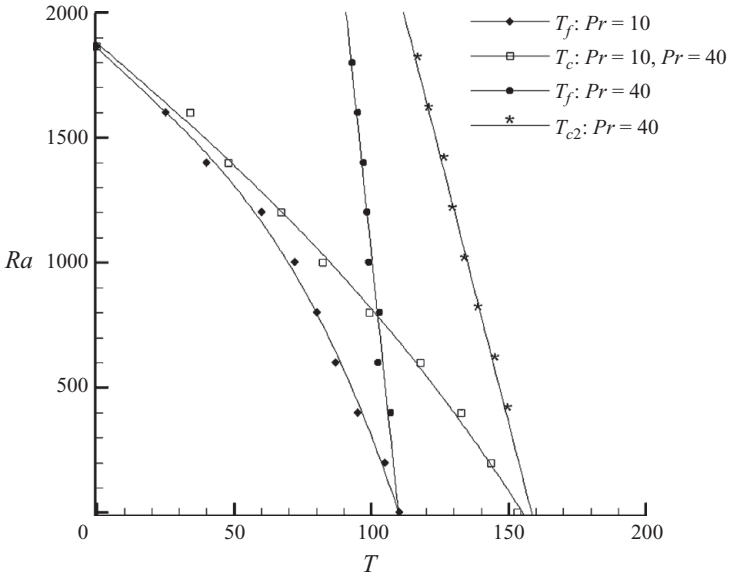

FIGURE 4. Instability thresholds for $Pr = 10$ and $Pr = 40$.

Close to the instability threshold, the perturbations of every physical quantity f grow according to the exponential law $f = f_0 e^{\sigma t}$. The growth rate σ is positive above the instability threshold and negative below it. If we let the system evolve from rest, the tiny numerical fluctuations always present suffice to induce motion. After an initial period of latency (typically 10 units of non-dimensional time) for which the velocity is very small and varies erratically, a first interval of exponential growth is observed. For a given L and a given T, we determine the growth rate of the perturbations in this interval, which is directly related to linear perturbations. A linear fit of the values of σ versus T gives the critical value of T which corresponds to $\sigma = 0$. Following this procedure, and as a test of the overall code, we have been able to reproduce the main results obtained in Atten & Moreau (1972).

Equation (11) means that a straight line separates the stable region from the unstable region for small-amplitude perturbations. However, one of the differences between the thermal and electrical instabilities is the wavenumber of the most unstable mode. For $Ra = 0$, the pure electrical problem, and for strong injection ($C = 10$), the expected width of the convective roll for small-amplitude motion is 0.614 whereas, for the pure thermal problem ($T = 0$), it is 1.0. This variation of the width of the convective rolls and hence of the wavenumber is not taken into account in the analytical model, since L is fixed. This variation results in a deviation of the critical line from a straight one. In order to deal with this problem of non-constancy of the most unstable wavenumber we have chosen a domain of computation of large L ($L = 10$). With such a length, the system is less constrained and can evolve freely towards the most unstable mode.

For different values of Ra and for two values of Pr, we have plotted the critical values of T defining the small-amplitude and finite-amplitude criteria for which the growth rate is zero: T_c or T_{c2} and T_f. In this diagram (figure 4), below the line corresponding to the finite-amplitude criteria labelled T_f, there is no motion and the rest state is stable. Above the lines T_c or T_{c2}, there is always motion with a maximum velocity greater than the ion drift velocity. Between both lines, there is hysteresis and we get motion or not depending on the previous value of T.

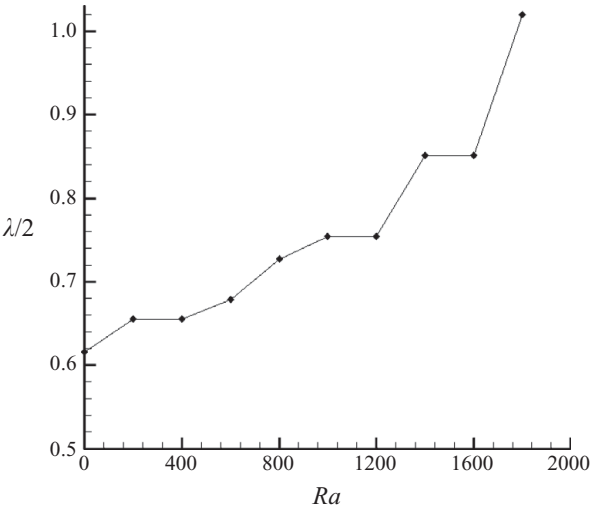

FIGURE 5. Wavelength versus Rayleigh number for Ra and T close to the critical line.

In these computations, the values of the other parameters are fixed ($C = 10$ and $M = 10$). The computed critical line deviates, as expected, from a straight line. The number of rolls observed when the velocity pattern is established varies along the line. In order to have a closer look at this variation, we made some simulations for values of T and Ra near the critical line. Starting from a rest state, the system evolves freely towards a certain number of rolls. The width of the rolls corresponds in fact to the half-critical wavelength $\lambda/2$ of the most unstable mode. In figure 5, $\lambda/2$ is plotted versus Ra and as expected it varies from 0.615 for $Ra = 0$ to 1.01 for $Ra = 1800$ whereas the theoretical corresponding values are 0.614 and 1.

The way λ depends on Ra shows some steps (observe the values at $Ra = 200$ and 400 or $Ra = 1400$ and 1600) due to the fact that only an integer number of rolls is allowed. Increasing the value of L, which is here equal to 40, these steps tend to disappear.

4.3. *Finite-amplitude behaviour*

The diagram for the small-amplitude criterion (values of T_c) plotted in figure 4 has already been presented by Castellanos & Velarde (1981) and Castellanos *et al.* (1984*a*), using a linear perturbation analysis of the equations. Our numerical code allows us to explore the finite-amplitude behaviour as well. Again, we expect to encounter a transition between the pure electrical and the pure thermal behaviours.

Figure 6 shows the results for three different values of the Rayleigh number for $Pr = 10$ (as before $C = 10$ and $M = 10$ are fixed). We have marked with arrows the small and finite-amplitude criteria, in order to make clear the hysteresis loop. As expected, the hysteresis loop reduces its amplitude as we increase the Rayleigh number. We must bear in mind that for $T = 0$ the bifurcation becomes supercritical and there is no hysteresis.

4.4. *Hysteresis loop on varying Ra*

Looking at figure 4, for $Pr = 10$, the question arises whether it would be possible to obtain a hysteresis loop by varying the Rayleigh number instead of the electrical parameter T. It seems clear that the only thing that is necessary is to keep T constant, but different from zero, and to vary the Rayleigh number in such a way as to cross

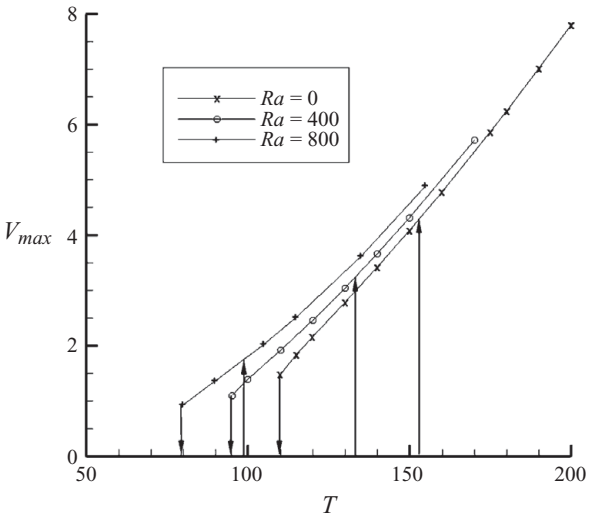

FIGURE 6. V_{max} versus T for three different values of Ra.

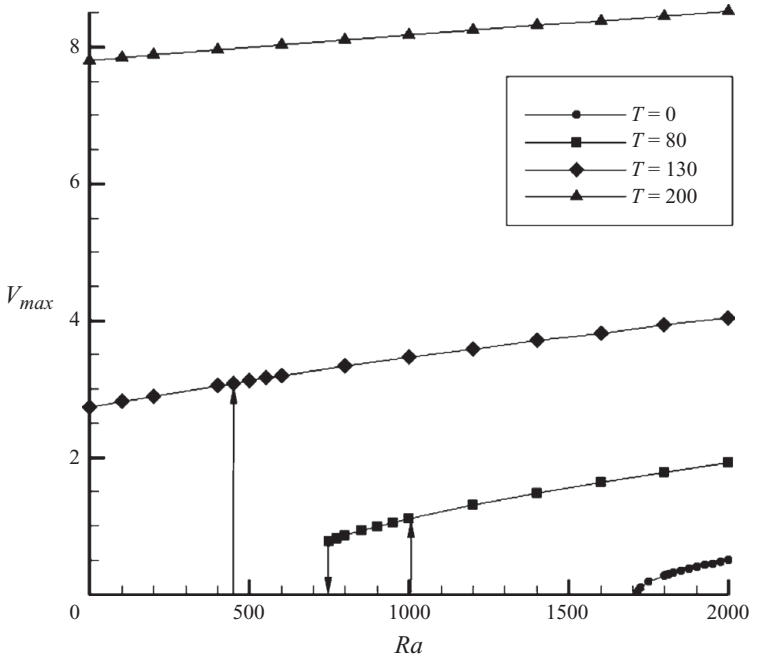

FIGURE 7. V_{max} versus Rayleigh number for four different values of T and for $Pr = 10$.

the critical line in a direction parallel to the Ra axis. On figure 7 we have plotted the evolution of V_{max} versus Rayleigh number for different values of T.

These results are consistent with the ones shown in figure 4. Depending on the value of T, there are one, two or no critical values of Ra. Although the subcritical character of the bifurcation is due to the presence of the electric force, we think it is remarkable to have found this type of bifurcation by adjusting only the Rayleigh number, that is to say, the temperature gradient.

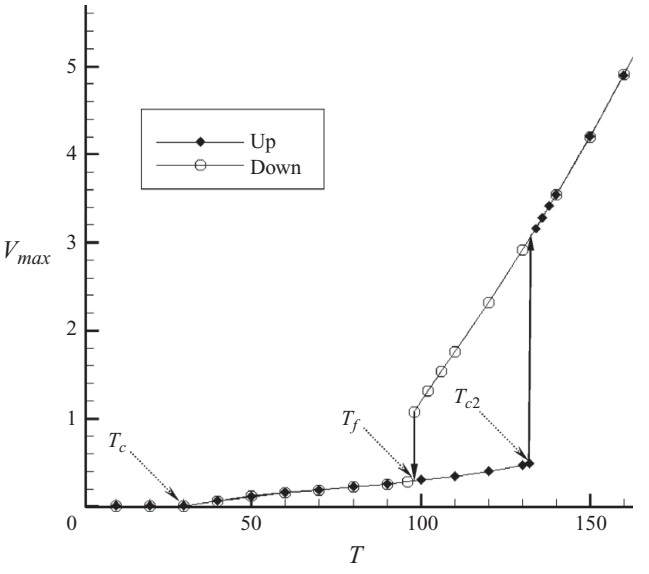

FIGURE 8. V_{max} versus T; $Ra = 1400$, $Pr = 40$.

4.5. *Supercritical behaviour*

If we increase the value of Pr, we expect to observe supercritical bifurcations for some value of Ra. Figure 8 shows the evolution of V_{max} as a function of T for $Ra = 1400$ and $Pr = 40$. We observe three critical values. At T close to 30, there is a first bifurcation, which is supercritical. This value of T, named T_c, is the small-amplitude critical value and is the same as predicted by (11). This value does not depend on Pr. Increasing T, we find another bifurcation at $T = 134$. We label this second critical value as T_{c2}. Decreasing the value of T a hysteresis loop is traced and another critical value T_f is found where the velocity returns to the lower branch. To sum up, figure 4 shows the main features qualitatively predicted by the analytical model presented in § 3.1.

The system is unstable for values of T and Ra above a line that does not depend on Pr and that is close to the straight line $Ra/Ra_c + T/T_c = 1$. For small values of Pr, the coefficient of A^2 in (11) is always positive and the bifurcation has a subcritical character. There are two thresholds and a hysteresis loop associated, as predicted by the schematic plot of figure 3(a). This is the situation for $Pr = 10$. Increasing the value of Pr introduces the possibility of having supercritical bifurcations. This is the case for $Pr = 40$, but even in this case, if Ra is small enough, the bifurcation is still subcritical. Indeed for $Ra < 400$ there are only two critical values of T: T_f and T_c (see figure 9). The transition is similar to that of figure 6 obtained for $Pr = 10$. It is still consistent with the pattern of figure 3(a). For $Ra > 400$ and $Pr = 40$ the product $Pr\,Ra$ is high enough to make the coefficient negative. Our analytical model predicts the existence of three critical values: T_f, T_c and T_{c2}. This behaviour corresponds now to the pattern of figure 3(c). In that case T_f can be smaller or greater than T_c, depending on Ra as clearly depicted in figures 10 and 11. These critical values can be found in figure 4 as well.

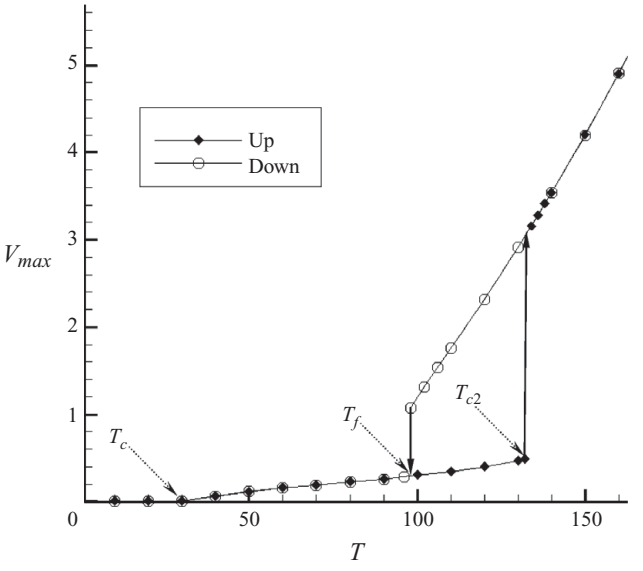

FIGURE 9. V_{max} versus T, $Ra = 200$, $Pr = 40$.

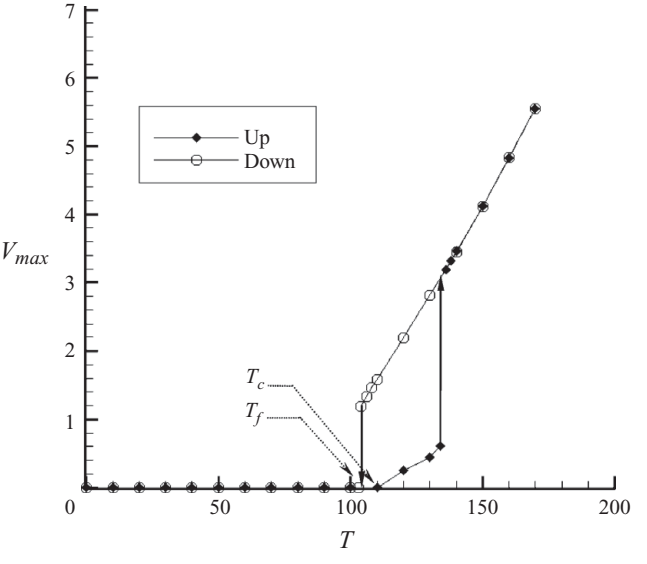

FIGURE 10. V_{max} versus T; $Ra = 600$, $Pr = 40$ case: $T_f < T_c$.

5. Electro-convection and heat transfer

In this section, several numerical simulations have been conducted in order to quantitatively measure the influence of electro-convection on heat transfer. The length of the cavity is $L = 10$ with symmetrical boundary conditions on the lateral walls. The results give 16 convective cells. A well-developed convective state is reached after a transition time: the non-stationary state starts for given values of T depending on M, C, Pr and Ra and then the Nusselt number fluctuates more or less around a mean value with a given frequency and amplitude (oscillatory regime). Figure 12 shows the

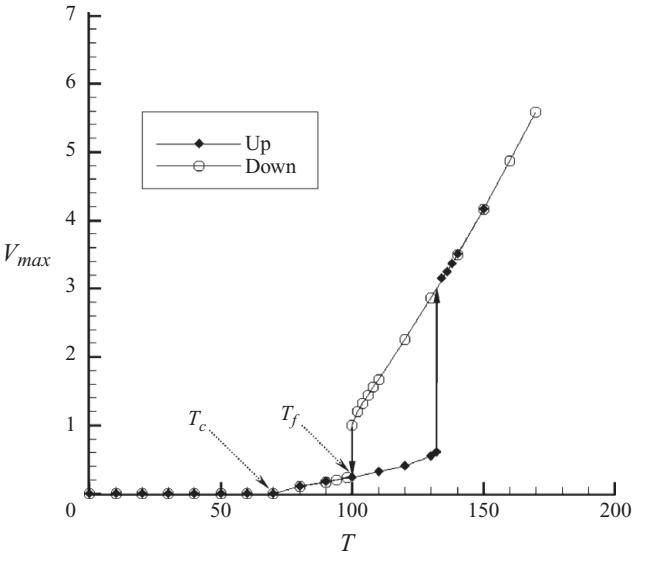

FIGURE 11. V_{max} versus T; $Ra = 1000$, $Pr = 40$ case: $T_f > T_c$.

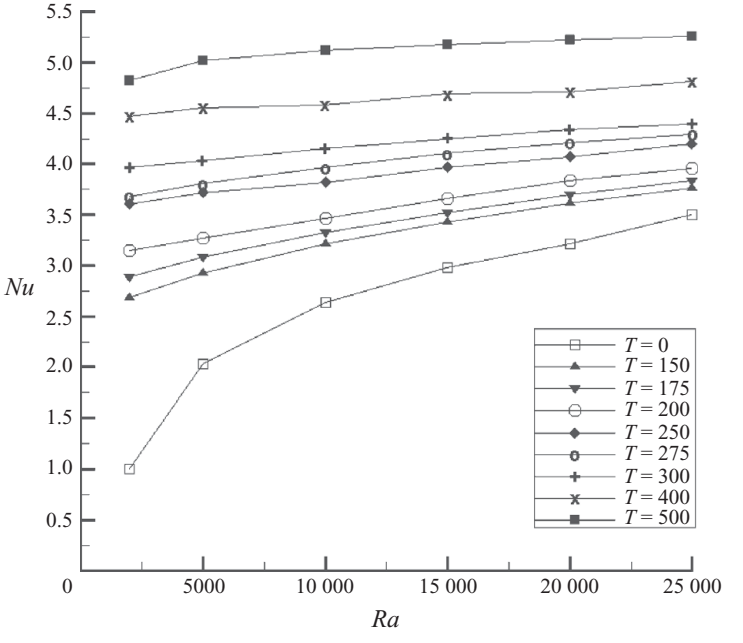

FIGURE 12. Mean Nusselt number for different values of T and Rayleigh number. $C = 10$ and $M = 10$.

mean value of the Nusselt number for different Ra and T. One can clearly see that above $T = 250$ the electrical forces dominate the heat transfer and for $T = 500$ the Nusselt number does not depend on Ra.

In some earlier works (Atten *et al.* 1988; McCluskey *et al.* 1991), the authors give experimental results that demonstrate that electro-convection induced by unipolar injection increases heat transfer. They use bare electrodes and silicone oil doped with

a suitable salt that produces a controlled and rather weak injection (C between 0.15 and 0.55). In McCluskey, Atten & Pérez (1988, figure 3), the Nusselt number is plotted as a function of the Rayleigh number, for different values of the applied voltage. Above a voltage of 6 kV the Nusselt number does not depend on the Rayleigh number, which means that the motion is completely dominated by the electrical forces. For higher potentials, the Nusselt number can be 10 times or more that without electric forces. Even if in our simulation the injection level C was 10, instead of less than 1 as in the mentioned experiments, both approaches give the same tendency: the electrical forces increase the heat transfer and from a certain value of the electrical parameter T they completely dominate the heat transfer, which does not depend on Ra any longer. The fact that the value of C is not the same is not really important here: if the electric forces dominate the heat transfer for small C (small influence from electric field), they will also dominate it for high C (great influence from electric field), which is the case in our simulations. Our code is therefore able to qualitatively reproduce the enhancement of heat transfer due to electro-convection and it could be a valuable tool for evaluating the efficiency of different geometrical configurations for heat exchanger designs.

6. Conclusion

In this paper, we have presented a finite-volume numerical modelling that solve the whole set of partial differential equations associated with the electro-thermo-convective phenomena. This set of coupled equations includes the Navier–Stokes equations, the charge density conservation equation, Poisson's equation for potential and the energy equation. The code has been used to study the stability of a dielectric liquid layer subjected to the simultaneous action of an electric field and a destabilizing temperature gradient with unipolar injection of electric charges from the lower hot electrode. We have obtained the curve in the plane Ra–T corresponding to the instability limit, which separates the linearly unstable region from the stable one and which deviates from a straight line. This deviation is a consequence of the variation of the most unstable wavenumber from one corresponding to a pure electrical problem ($Ra = 0$) to one corresponding to a pure thermal problem ($T = 0$). For fixed values of the Rayleigh number, we have found hysteresis loops in the variation of the velocity with T. They are a conspicuous characteristic of the unipolar injection problem. We have also determined the line associated with the finite-amplitude stability criterion connected to the hysteresis loop in the Ra–T plane. The presence of the electric force makes possible the hysteretic behaviour of the liquid flow velocity when the Rayleigh number varies, which is not the case in the pure thermal problem. An analytical model has been developed to understand the appearance of subcritical or supercritical bifurcations depending on the value of Pr or M. With the insights provided by this model and confirmed by numerical results, we have been able to find a subcritical bifurcation by varying the Rayleigh number which coexists with supercritical behaviour when varying the electrical parameter T. These behaviours are opposite to the ones expected for the corresponding pure problems. Finally, we have evaluated the heat transfer enhancement due to electro-convection. We have demonstrated that the electric force may enhance heat transfer and that the Nusselt number becomes almost independent of Rayleigh number for high enough values of T. Our results are in good qualitative agreement with available experimental data.

REFERENCES

Atten, P. & Lacroix, J. C. 1979 Non linear hydrodynamic stability of liquids subjected to unipolar injection. *J. Méc.* **18**, 469–510.

Atten, P., McCluskey, F. M. G. & Pérez, A. T. 1988 Electroconvection and its effect on heat transfer. *IEEE Trans. Electr. Insul.* **23**(4), 659–667.

Atten, P. & Moreau, R. 1972 Stabilité électrohydrodynamique des liquides isolants soumis à une injection unipolaire. *J. Méc.* **11** (3), 471–521.

Bryan, J. E. & Seyed-Yagoobi, J. 1997 Heat transport enhancement of monogroove heat pipe with electrohydrodynamic pumping. *J. Thermophys. Heat Transfer* **11**(3), 454–460.

Bryan, J. E. & Seyed-Yagoobi, J. 2001 Influence of flow regime, heat flux, and mass flux on electrohydrodynamically enhanced convective boiling. *J. Heat Transfer* **123** (2), 355–367.

Castellanos, A. 1991 Coulomb driven convection in electrohydrodynamics. *IEEE Trans. Electr. Insul.* **26**, 1201–1215.

Castellanos, A., Atten, P. & Pérez, A. T. 1987 Finite amplitude electroconvection in liquid in the case of weak unipolar injection. *PhysicoChem. Hydrodyn.* **9** (3/4), 443–452.

Castellanos, A., Atten, P. & Velarde, M. G. 1984*a* Oscillatory and steady convection in dielectric liquid layers subjected to unipolar injection and temperature gradient. *Phys. Fluids* **27**, 1607–1615.

Castellanos, A., Atten, P. & Velarde, M. G. 1984*b* Electrothermal convection: Felici's hydraulic model and the Landau picture of non-equilibrium phase transitions. *J. Non-Equilib. Thermodyn.* **9**, 235–244.

Castellanos, A. & Velarde, M. G. 1981 Electrohydrodynamic stability in the presence of a thermal gradient. *Phys. Fluids* **24**, 1784–1786.

Chicón, R., Castellanos, A. & Martín, E. 1997 Numerical modelling of Coulomb-driven convection in insulating liquids. *J. Fluid Mech.* **344**, 43–66.

Chicón, R., Castellanos, A. & Pérez, A. T. 1999 Transient electrohydrodynamic stability of dielectric liquids subjected to unipolar injection. *Inst. Phys. Conf. Ser.* **163**, 157–160.

Davis, S. F. 1984 TVD finite difference schemes and artificial viscosity. *ICASE Rep.* 84-20, *NASA CR*-172373. NASA Langley Research Center.

Felici, N. 1969 Phénomènes hydro et aérodynamiques dans la conduction des diélectriques fluides. *Rev. Gén. Electr.* **78**, 717–734.

Felici, N. 1972 D.C. conduction in liquid dielectrics Part II. Electrohydrodynamic phenomena. *Direct Curr.* **2**, 147–165.

Fortin, M. & Glowinski, R. 1983 *Augmented Lagrangian Methods.* North-Holland.

Gaskel, P. H. & Lau, A. K. C. 1988 Curvature-compensated convective transport: SMART, a new boundedness-preserving transport algorithm. *Intl J. Numer. Methods Fluids* **8**, 617–641.

Godunov, S. K. 1959 A Difference scheme for numerical computational of discontinuous solution of hydrodynamic equations. *Math. Sb.* **47**, 271–306. Translated in US Joint Publications Research Service, *JPRS* 7226 (1969).

Grassi, W. & Testi, D. 2006 Heat transfer enhancement by electric fields in several heat exchanger regimes. *Ann. N. Y. Acad. Sci.* **1077** (1), 527–569.

Lin, C.-W. & Jang, J.-Y. 2005 3D numerical heat transfer and fluid flow analysis in plate-fin and tube heat exchangers with electrohydrodynamic enhancement. *Intl J. Heat Mass Transfer* **41**, 583–593.

Martin, P. J. 1982 Electrohydrodynamic instabilities in a horizontal layer of dielectric liquid heated from above and subjected to a DC electric field. Doctoral thesis, University of Bristol, Bristol, UK.

Martin, P. J. & Richardson, A. 1982 Overstable electrothermal instabilities in a plane layer of dielectric liquids. *J. Eectrostat.* **12**, 435.

McCluskey, F. M. G., Atten, P. & Pérez, A. T. 1991 Heat transfer enhancement by electroconvection resulting from an injected space charge between parallel plates. *Intl J. Heat Mass Transfer* **34**, 2237.

Patankar, S. V. 1980 *Numerical Heat Transfer and Fluid Flow.* McGraw-Hill.

Pérez, A. T., Atten, P., Malraison, B., Elouadi, L. & McCluskey, F. M. G. 1988 Heat transfer augmentation induced by electrically generated convection in liquids. In *Experimental Heat Transfer, Fluid Mechanics and Thermodynamics* (ed. R. Shah, E. Ganic & K. Yang), pp. 941–947. Elsevier.

Pontiga, F. & Castellanos, A. 1992 The onset of electrothermal convection in non polar liquid layers on the basis of dissociation-injection conductivity model. *IEEE Trans. Ind. Appl.* **IA28**, 520–527.

Pontiga, F. & Castellanos, A. 1994 Physical mechanism of instability in a liquid layer subjected to an electric field and a thermal gradient. *Phys. Fluids* **6** (5), 1684–1701.

Richardson, A. T. 1988 A hydraulic model of electrothermal convection in a plane layer of dielectric liquid. *PhysicoChem. Hydrodyn.* **10** (3), 355–367.

Rodrigues, L., Castellanos, A. & Richardson, A. 1986 Stationary instabilities in a dielectric liquid layer subjected to an arbitrary unipolar injection and adverse thermal gradient. *J. Phys.* D*: Appl. Phys.* **19**, 2115–2122.

Suman, B. 2006 A steady state model and maximum heat transport capacity of a electro-hydrodynamic augmented micro-grooved heat pipe. *Intl J. Heat Mass Transfer* **49**, 3957–3967.

Traoré, Ph. 1996 Contribution numérique à l'étude des transferts couplés de quantité de mouvement de chaleur et de masse dans un jet semi-confiné. PhD thesis, University of Toulouse III, France.

Tsai, P., Daya, Z. A., Deyirmenjian, V. B. & Morris, S. W. 2007 Direct numerical simulation of supercritical annular electroconvection. *Phys. Rev.* E **76**, 026305.

Vázquez, P. A., Georghiou, G. E. & Castellanos, A. 2006 Characterization of injection instabilities in electrohydrodynamics by numerical modelling: comparison of particle in cell and flux corrected transport methods for electroconvection between two plates. *J. Phys.* D*: Appl. Phys.* **39**, 2754–2763.

Vázquez, P. A., Georghiou, G. E. & Castellanos, A. 2008 Numerical analysis of the stability of the electro-hydrodynamic (EHD) electroconvection between two plates. *J. Phys.* D*: Appl. Phys.* **41**, 1–10.

Worraker, W. & Richardson, A. 1979 The effect of temperature-induced variations in charge carrier mobility on a stationary electrohydrodynamic instability. *J. Fluid Mech.* **93**, 29.

Worraker, W. & Richardson, A. 1981 A nonlinear E stability analysis of a thermally stabilized plane layer of dielectric liquid. *J. Fluid Mech.* **109**, 217–237.